Cancer Nanotechnology

RESEARCH Open Access

Two birds with one stone: triple negative breast cancer therapy by PtCo bimetallic nanozyme coated with gemcitabine-hyaluronic acid-polyethylene glycol

Majid Sharifi[1,2*], Rasoul Kheradmandi[1,2*] and Morteza Alizadeh[2*]

*Correspondence:
Sharifi@shmu.ac.ir;
rasoulkheradmandi@gmail.com;
alizadeh.m@shmu.ac.ir

[1] Student Research Committee, School of Medicine, Shahroud University of Medical Sciences, Shahroud, Iran
[2] Department of Tissue Engineering, School of Medicine, Shahroud University of Medical Sciences, Shahroud, Iran

Abstract

For the treatment of triple-negative breast cancer (TNBC), without expression of estrogen, progesterone and HER2 receptors, specific treatment guideline is still under criticism, especially in tumor hypoxia. But assuming the molecular similarity of TNBC with breast cancer gene-1-related cancers, gemcitabine may be used in TNBC treatment on the nanozyme platform combined with photodynamic therapy (PDT). After designing the nanozyme with four components, platinum–cobalt: with catalase/peroxidase capabilities, hyaluronic acid: nanozyme targeting by interacting with CD44 receptor, poly[ethylene glycol]: water-soluble macromolecule for immune escape, and Gem: antitumor drug, its physicochemical properties was investigated by thermogravimetric, X-ray diffraction and energy dispersive X-ray, and therapeutic effects in in vitro and in vivo. The results show that platinum–cobalt@gemcitabine-hyaluronic acid-polyethylene glycol (PtCo@Gem-HA-PEG) especially synergized with PDT has high toxicity on 4T1 cells and tumor by enhancing the catalase-/peroxidase-like activities to produce O_2, $O_2^{\bullet-}$ and $^{\bullet}OH$, and increase the intracellular free radicals. PtCo@Gem-HA-PEG inhibits tumor development by increasing drug accumulation in the tumor and enhancing apoptotic mechanisms through synergistic activity with PDT. Nevertheless, the major organ damage confirmed by the histological method in the long-term application of PtCo@Gem-HA-PEG, makes their application challenging due to permanent catalytic activity. However, results of improved drug permeability based on reduced hypoxia, higher drug retention, and enzyme-like activity that could be synergized with other therapeutic approaches like a PDT, have made their use attractive. Hence, this study provides a promising path in the TNBC treatment by nanozymes, which requires further toxicological investigations.

Keywords: Triple-negative breast cancer, Nanozyme, Photodynamic therapy, Drug delivery, Gemcitabine

Graphic Abstract

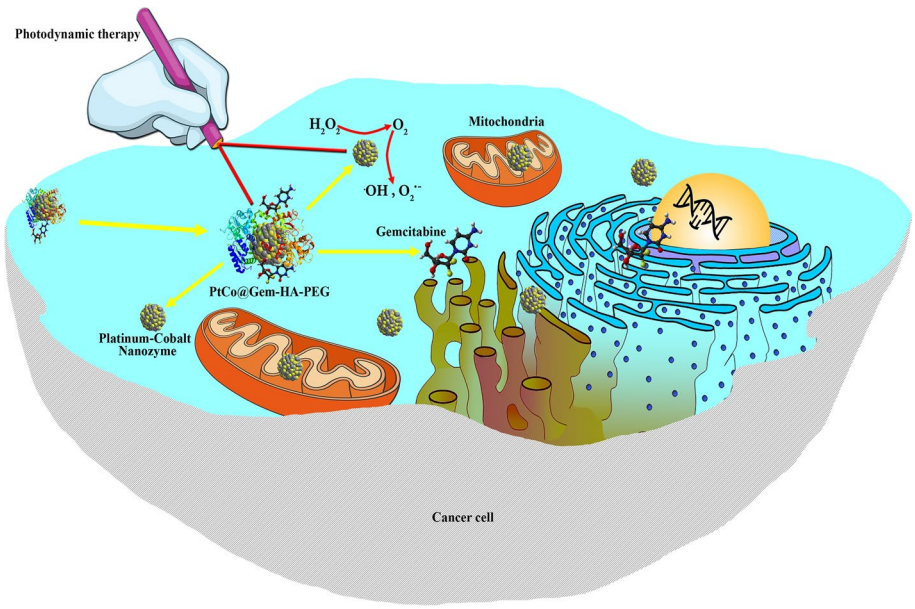

Introduction

Triple-negative breast cancer (TNBC) with a lack of expression of estrogen, progesterone, and human epidermal growth factor 2 receptors comprises approximately 15 to 20% of breast cancer cases (Alsughayer et al. 2022; Sharifi et al. 2021), which generally have deleterious mutations in breast cancer gene-1 (Lønning et al. 2022). The higher risk of recurrence of TNBC compared to other subtypes of breast cancer and their very poor prognosis has made the treatment path very challenging. Due to late diagnosis and inefficiency of chemotherapy activities, surgery is considered the most important TNBC treatment strategy (Alsughayer et al. 2022; Wang et al. 2022). Nevertheless, the therapeutic hopes resulting from combined approaches such as the integration of chemotherapy with photo-therapy, thermal-therapy, radio-therapy, etc., have directed attention towards more non-invasive activities (Zeng et al. 2022; Wu et al. 2022).

Although drugs such as anthracycline, taxanes, docetaxel and cisplatin are considered to be the most important chemotherapy drugs in the TNBC treatment (Zhu et al. 2022; Iqbal et al. 2021), the statistical trend based on Scopus, Web of Science and PubMed reports (Fig. 1) shows that in the last 10 years the use of gemcitabine (Gem) has received attention due to less side effects and improvement of treatment efficiency up to 79% when combined with other drugs (Wengner et al. 2020; Pellegrino et al. 2021; Yardley et al. 2018; Fan et al. 2017). For instance, it was determined that the timed release of doxorubicin and Gem with hyaluronic acid (HA) resulted in 2.5-fold inhibition of orthotopic 4T1 tumor invasion in vivo compared to free doxorubicin and Gem (Vogus et al. 2017). In this regard, Xie et al. (2021) showed that the antitumor effect of birinapant, a mitochondria-derived caspase activator, causes anti-proliferative activity in remaining TNBC cells in addition to cell death. They demonstrated that Gem has a strong

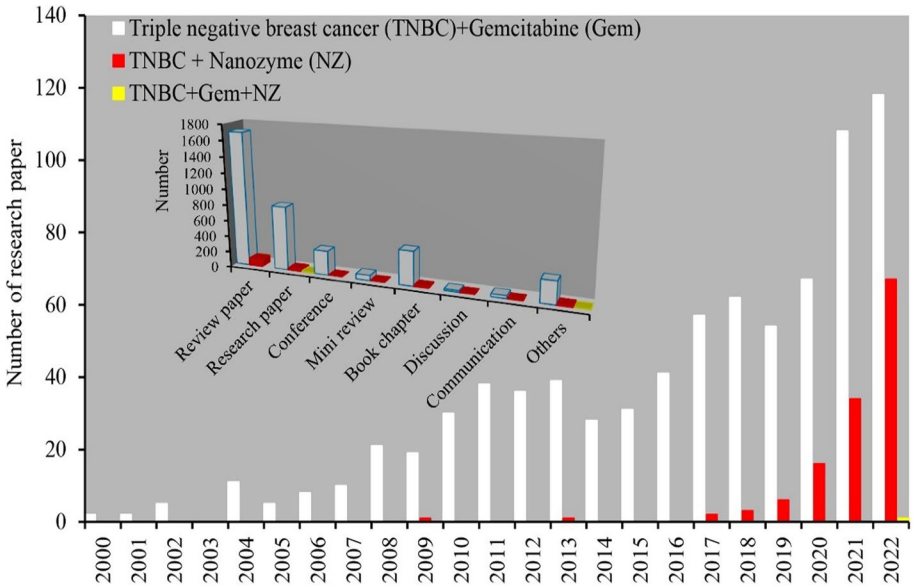

Fig. 1 Chronological increase in the scientific attention on nanozyme for triple-negative breast cancer therapy, based on reports from Scopus, PubMed, and Web of Science sites

synergistic effect with birinapant compared to cisplatin, paclitaxel, Voxtalisib, dasatinib, and erlotinib to induce caspase-mediated apoptosis (Vogus et al. 2017; Xie et al. 2021). However, drug resistance in long-term use of Gem and systemic toxicities in high doses have reduced its therapeutic capabilities in clinical activities (Paroha et al. 2021). Therefore, continuous monitoring is still needed to reveal the therapeutic effects of Gem in synergy with other therapeutic approaches to reduce toxicity via reducing the prescribed dosage without reducing the efficacy and enhancing the penetration of Gem into cancer cells along with their targeted administration in clinical activities.

Since TNBC has a relatively acidic environment and a high concentration of H_2O_2, the presence of pH-sensitive nanozymes (NZ) and their retention in the tumor through increased permeability of vessels and defects in the lymphatic system can enhance drug delivery and retention, reduce hypoxia and the radical's generation in a targeted way (Sharifi et al. 2022; Xing et al. 2021). By strengthening catalytic approaches in order to produce radicals, NZ enables greater penetration of medicinal compounds or induction of apoptosis in cancerous cells (Falahati et al. 2022; Mansur et al. 2020; Bao et al. 2022). In addition to the ability of targeted drug delivery with enzyme-like activities, these compounds are very beneficial due to their high stability, cheapness and resistance to environmental conditions (Bao et al. 2022; Sharifi et al. 2020). For example, Cen et al. (2022) were able to effectively reduce primary tumor growth and metastatic activity of breast cancer through the increase of reactive oxygen species (ROS) based on the peroxidase-like activity of palladium–ruthenium bimetallic NZ enhanced by photodynamic therapy (PDT). In this regard, in a mice model, Nie et al. (2022) revealed that the use of platinum NZ loaded on iron nanospheres containing 5-fluorouracil reduces the size of breast tumors. They related the reduction of tumor volume to the intrinsic function of NZ including peroxidase and catalase through the increase of ROS, and the hypoxia reduction for greater drug penetration. Recently, Xi et al. (2022) enhanced the healing

process by loading Gem in carbon NZ doped with nitrogen by improving the peroxidase-like activity and the formation of •OH along with reducing the resistance to Gem in tumor cells. However, it seems that the intrinsic activities of single-element NZ are challenged by the moderately acidic tumor microenvironment. Hence, Bao et al. (2021) by designing a bimetallic platinum–cobalt (PtCo) NZ with high radiation absorption for damage DNA especially by Pt, and double catalase activity to convert H_2O_2 to O_2 significantly reduced the growth of lung tumor. Meanwhile, it has been revealed that the use of photo-therapy, thermal-therapy and radio-therapy approaches effectively improve the antitumor activities of single or multi-metallic NZ (Jiao et al. 2021; Gao et al. 2020; Hou et al. 2022). For instance, Wu et al. (2022) with synergy of PDT and chemo-therapy based on manganese oxide NZ containing doxorubicin not only improved drug delivery through modifying the membrane of TNBC cells and ROS to induce apoptosis, but also provided a suitable opportunity for imaging by reducing hypoxia. Similarly, it was determined that the use of PDT effectively increases the rate of O_2 release by CeO_2 NZ containing Cinobufagin (Zeng et al. 2022). Sustained supply of O_2 led to greater drug penetration, reduced cell migration, and reduced TNBC tumor size in a mice model.

Herein, bimetallic PtCo NZ coated with Gem-HA-poly[ethylene glycol] (PEG) was designed to reduce TNBC growth based on the synergy of chemotherapy and enzyme-like activity enhanced by PDT. HA-PEG coating was used for immune escape in blood circulation and the possibility of NZ retention in cancer cells. An attempt was made to provide an analysis of the effect of NZ in TNBC cells with peroxidase and catalase activities, by creating ROS and producing O_2 in a sustainable way to induce apoptosis and higher drug effectiveness, respectively. In theory, NZ designed with enzyme-like activity and drug delivery can increase the efficacy of Gem in the treatment of TNBC with lower toxicity and higher efficiency.

Materials and method

Materials

$H_2PtCl_6{\cdot}6H_2O$, $C_4H_6CoO_4{\cdot}4H_2O$ (99%), polyvinyl pyrrolidone (99%), and $NaBH_4$ (98%) were purchased from the Merck Company (Germany). Dulbecco's modified Eagle medium (DMEM) cell culture, MTT powder, and fetal bovine serum (FBS) were obtained from Gibco (Scotland). Hyaluronic acid (MW 10 kDa), NH2-poly[ethylene glycol]-SH (MW 1 kDa), and gemcitabine hydrochloride (Gem) were purchased from the Sigma Aldrich Company (USA). Tetra-methylbenzidine (TMB), and dimethyl sulfoxide (DMSO) were purchased from Aladdin Reagent. Rabbit anti-phospho-histone H2AX was purchased from Bioss. Ultrapure water was used throughout the experiment. Annexin V-FITC kit was obtained from Iq products, Poland. The BALB/c mice and 4T1 cells were purchased from Pasteur Institute (Tehran, Iran).

PtCo@Gem-HA-PEG NZ preparation

In order to synthesize PtCo NZ, two separate solutions were generated (Wei et al. 2020). The first solution: 24 mg of $C_4H_6CoO_4{\cdot}4H_2O$ as cobalt source was dissolved with 400 mg of PVP in 120 mL of deionized water to get a red solution. Then, 100 mL of $NaBH_4$ solution (4 mg/mL) was added to the above solution to produce a black suspension during 20 s. The second solution: $H_2PtCl_6{\cdot}6H_2O$ solution (0.25–1.3 mg/mL) was added to

80 mL of deionized water. At the end, the second solution is added to the first solution and stirred until the gas bubbles are removed. The final product was collected by centrifugation and washed several times with deionized water. The PtCo NZ was stored at 4 °C.

To provide a Gem-HA-PEG coating on the PtCo NZ for drug delivery, stealth and targeting, first of all, 2.67 mg of carbonyldiimidazole was dissolved in 200 µL of *N*,*N*-dimethylformamide. Then, 50 mg of HA was dissolved in 0.5 mL of deionized water containing the above solution for 2 h at 21 °C. After the activation of HA, 25 mg of PEG dissolved in 100 µL of deionized water was added to the above solution with 10 µL of trimethylamine. In the following, to load Gem onto HA-PEG, HA-PEG (200 mg) was dissolved in 10 mL of phosphate-buffered saline (PBS) (pH = 5.5). Then, Gem (60 mg), EDC (60 mg) and NHS (52 mg) were added to the above solution and reacted at 25 °C for 24 h under a nitrogen atmosphere. Finally, the products were purified using a PD-10 column and the thiol-containing Gem-HA-PEG was obtained by vacuum distillation using a rotary evaporator. Previously, to optimize the loading of Gem in HA-PEG, different concentrations of Gem with a weight ratio of 15, 30, 45, 60 and 75% compared to HA-PEG were investigated.

To assemble PtCo@Gem-HA-PEG NZ, 3 mL of PtCo NZ (30 mg) was added to 30 mL of chloroform containing 30 mg/mL Gem-HA-PEG containing thiol group. The mixture was stirred at room temperature for 8 h and then collected by centrifugation (at 10,000 rpm for 5 min). The obtained PtCo@Gem-HA-PEG NZ was washed by ethanol and water. Then, PtCo@Gem-HA-PEG NZ was dispersed in 4 mL deionized distilled water and stored at 4 °C.

Drug concentration

Aggarwal et al. (2013) method was used to determine the loading efficiency (%) and loading capacity (%) of Gem in HA-PEG. Briefly, 5 mg of Gem-HA-PEG was dissolved in 1 mL of acetonitrile and 4 mL of PBS (pH = 7.4). Then, the mixture was stirred at room temperature for 24 h. The supernatant obtained from centrifugation (12,000 revolutions for 15 min) was analyzed by UV–visible spectrometry at 270 nm. The outcomes were reported by the following 1 and 2 equations:

$$\text{Loading efficacy} = \frac{[\text{initial amount of Gem} - \text{amount of Gem in supernatant}]}{\text{initialamountofGem}}, \quad (1)$$

$$\text{Loading capacity} = \frac{[\text{initial amount of Gem} - \text{amount of Gem in supernatant}]}{\text{amount of Gem} - \text{loaded PEG} - \text{HA}}. \quad (2)$$

PtCo@Gem-HA-PEG NZ characterization

The morphology and size of the prepared PtCo NZ were observed on a SEM (Scanning electron microscopy: JEOL-6700, Japan). Energy dispersive X-ray (EDX) spectrometer study was carried out on a JEOL JEM2010 electron microscope at 100 kV. Transmission electron microscopy (TEM: HRTEM, JEM-2010) images with an acceleration voltage of 100 kV were used to examine the morphological status of PtCo@Gem-HA-PEG NZ. Thermogravimetric analysis of the PtCo NZ and PtCo@Gem-HA-PEG NZ were investigated by a thermogravimetric analyzer (TG209-F3, USA) under argon with a heating

rate of 10 °C/minute. Also, Zetasizer Nano ZS90 (Malvern Instruments, UK) was applied to assess the hydrodynamic size distribution. The crystal phase of the PtCo NZ and PtCo@Gem-HA-PEG NZ were determined using XRD analysis with Cu Kα radiation (λ = 1.5418 Å) at 40 kV and 50 mA.

O_2 generation and catalase-mimic activity assays

The O_2 concentration in aqueous solutions was quantized by an oxygen electrode with multi-parameter analysis (JPSJ-606L, China). In order to investigate the catalytic ability of NZ, H_2O_2 (100 μM) was added to 30 mL of O_2-free water, and then the mixture was placed in a three-necked flask (50 mL). The O_2 electrode probe was inserted into the flask. When the concentration of O_2 in the initial solution reached equilibrium, 20 μg of PtCo NZ and PtCo@Gem-HA-PEG NZ with and without laser irradiation (660 nm: 100 mW/cm^2) was injected into system through a syringe. O_2 concentration was recorded every 50 s for 5 min.

In addition, to determine the catalase activity of NZ, 20 μg/mL of PtCo NZ and PtCo@Gem-HA-PEG NZ were mixed with 1 mL of PBS buffer (pH = 6.5) and 20 mM H_2O_2. After 10 min of incubation at 37 °C, the H_2O_2 concentration is scaled according to the decrement of absorbance at 240 nm, which indicates the catalase activity of NZ with and without laser irradiation (660 nm: 100 mW/cm^2).

Peroxidase-like activity assay and superoxide/hydroxyl radical detection

For the purpose to investigate the peroxidase performance of NZ with and without laser irradiation (660 nm: 100 mW/cm^2), TMB oxidation and absorption spectrum analysis at 652 nm by UV–Vis spectrophotometer were used. 20 μg/mL of PtCo NZ and PtCo@Gem-HA-PEG NZ were suspended in 30 mM PBS (pH = 6.5) and then TMB was added until the solution reached a final concentration of 800 μM. To create hypoxic conditions, N_2 gas was injected into the PBS solution to remove O_2 before adding NZ. In addition, the effect of pH (5–7.5), temperature (20–50 °C), and DMEM + FBS concentration (0–100 μg/mL) on PtCo@Gem-HA-PEG NZs peroxidase-like activity were measured for achieving the optimal conditions.

Hydroethidine and terephthalic acid were used to detect $O_2^{\bullet-}$ and $^{\bullet}OH$, respectively. By considering the oxidation of hydroethidine to ethidine in the presence of $O_2^{\bullet-}$ (emitting bright red fluorescence) and the conversion of terephthalic acid to 2-hydroxy terephthalic acid with unique fluorescence (at 430–435 nm) in the presence of $^{\bullet}OH$, quantity amounts were detected.

Drug release

The Gem release profile was measured by applying the dialysis bag. The 200 μg of PtCo@Gem-HA-PEG NZ was placed in a dialysis bag (MWCO 12,000). Next, dialysis bags were suspended in 50 mL of PBS solution with pH of 7.4, 6.5 and 6.0 and 1 mM H_2O_2. The solutions were continuously shaken at 37 °C at 180 r.p.m. 5 mL of the solution was taken from the tank for analysis at 0.01, 0.25, 0.50, 1, 1.5, 3, 6, 9, 12, 16 and 24 h, and the

same amount of the initial buffer was added to them. The Gem released was evaluated by UV spectroscopy at 260 nm. The Gem cumulative release was quantized based on Eq. 3:

$$\text{Cumulative drug release (\%)} = \frac{5 \times \sum_{i-1}^{n-1} C_i + 50 \times C_n}{\text{weight of Gem on PtCo@Gem} - \text{HA} - \text{PEG}} \times 100. \tag{3}$$

C_i and C_n refer to the of Gem concentration at time i and n, respectively.

In vitro trials

Cytotoxicity assay

The toxicity of Gem, PtCo NZ and PtCo@Gem-HA-PEG NZ with and without laser irradiation (660 nm: 100 mW/cm^2 for 10 min) was evaluated by MTT method on 4T1 cells. Briefly, 4T1 cells were seeded in 96-well plates at a density of 6000 cells/well (100 µL) in DMEM + 10% FBS and 1% penicillin/streptomycin, and incubated at 37 °C with 5% CO_2 and 1% O_2 (for mimicking the hypoxic environment) for 24 h. Then, different concentrations of Gem and NZ were added to the wells. In order to synergize chemotherapy with PDT, 4T1 cell samples were exposed to laser irradiation 6 h after incubation for 10 min. Then the samples were incubated again. The cells were subsequently incubated for 24 and 48 h in the CO_2 incubator at 37 °C with 5% CO_2 and 1% O_2 (for mimicking the hypoxic environment). In the following, 10 µL of MTT solution (5 mg/mL) was added to each well. Again, the plate was incubated for 4 h. By removing the culture medium and adding DMSO (100 µL) to each well, absorbance values were defined with a Bio-Rad microplate reader at 490 nm. Finally, the percentage of cell viability was evaluated by Eq. 4:

$$\text{Cell viability (\%)} = (\text{OD treated}/\text{OD control}) \times 100\%. \tag{4}$$

DNA double-strand breaks

For this purpose, 4T1 cells (15,000 cells/well) were seeded in a 24-well plate and incubated for 24 h at 37 °C and 5% CO_2 and 1% O_2 (for mimicking the hypoxic environment). Then, Gem (37.5 µg/mL), PtCo NZ (75 µg/mL), and PtCo@Gem-HA-PEG (75 µg/mL) were added to the 24-well plate with and without laser irradiation (660 nm: 100 mW/cm^2 for 10 min). Again, the samples were incubated in the incubator for 24 h with the hypoxic condition. Then, the immunofluorescence staining of γ-H2AX was carried out. So, the 4T1 cells were fixed (4% paraformaldehyde: 25 min) and 0.5% Triton X-100 (5 min) was used to penetrate the cells. Meanwhile, BSA was applied to prevent non-specific protein interactions. Ultimately, the 4T1 cells were incubated with γ-H2AX antibody (1:200) at 4 °C for 12 h. Next step, the FITC-labeled sheep anti-mouse secondary antibody (1:500) was added for 2 h at 37 °C with the hypoxic condition. Then, the coverslips were washed by PBS. In addition, cell nuclei were stained by Hoechst.

ROS and apoptosis assays

To assess intracellular ROS, 4T1 cells (2×10^5 cells/well) were treated with Gem, PtCo NZ and PtCo@Gem-HA-PEG NZ with and without laser irradiation (660 nm: 100 mW/

cm^2 for 10 min). The 4T1 cells were gathered in serum-free DMEM after incubation for 24 h with 5% CO_2 and 1% O_2 (for mimicking the hypoxic environment). In the following, DCFH-DA probe (10 μM) was added to the above suspension and incubated at 37 °C for 30 min in the dark. Fluorescent signals and fluorescent images were evaluated by flow cytometer and fluorescent microscope (Olympus, Japan), respectively. For imaging, 4T1 cells were washed (3 times) with serum-free DMEM.

Meanwhile, in order to estimate apoptosis, the 4T1 cells were seeded (2×10^5 cells/well) in six-well plates and incubated for 24 h in 5% CO_2 and 1% O_2 (for mimicking the hypoxic environment) at 37 °C. In the next step, 4T1 cells treated with Gem (37.5 μg/mL), PtCo NZ (75 μg/mL), and PtCo@Gem-HA-PEG (75 μg/mL) with and without laser irradiation (660 nm, 30 mW/cm^2 for 10 min) were incubated again for 24 h with the hypoxic condition. After that, the cells were collected (3000 g centrifugation for 3 min) and stained with 5 μL Annexin V-FITC at room temperature for 20 min and followed by 10 μL propidium iodide (PI) for 5 min in the dark. The samples were evaluated by using FACscan (BD Bioscience, USA).

In vivo trials

Animal model

All 6-week-old female Balb/c mice (23.1 ± 2.4 g) and their experiments were complied with the guideline of the Animal Care and Use Committee of Shahroud University of Medical Sciences. Thirty-two mice were randomly divided into four groups, including control, Gem (5 mg/kg), PtCo NZ (5 mg/kg), and PtCo@Gem-HA-PEG NZ (5 mg/kg) with and without laser irradiation (660 nm: 100 mW/cm^2 for 10 min). The mice were subcutaneously injected with 150 μL cell suspension (5×10^5 4T1 cancerous cells) to develop tumors. After 22 days, when the tumors reached $141.2 \pm 7.8\,mm^3$, the mice were treated with drug and NZ.

Gem blood concentration and hematology analysis

In order to evaluate the level of Gem in blood, HPLC (SPD-M20A, Japan) method was used. 0.50 mL of whole blood was collected at time intervals of 1, 2, 4, 6, 12, 24 and 48 h after the injection of Gem on days 1, 7 and 14. Then the plasma obtained from blood centrifugation at 4 °C for 15 min at 1600 r.p.m. was kept at − 20 °C. At the 21th, 28th, and 35th days, 8 h after Gem injection, blood samples (20 μL per blood sampling) were collected from mice and sent to the laboratory for analysis of alanine transaminase (ALT), aspartate aminotransferase (AST), alkaline phosphatase (ALP), creatinine (CRA), and blood urea nitrogen (BUN) after centrifugation at 4 °C for 15 min at 1600 r.p.m. The levels of ALT, AST, ALP, BUN and CRA were detected by ELISA kits (MyBioSource).

Body weight, PDT and tumor status

To survey the biosafety, the weight of the mice were measured every 7 days and any abnormal behavior of the mice were frequently considered. Furthermore, mice that were treated with PDT, their tumor site every 7 days were irradiated with a near-infrared light source with a power density of 100 mW/cm^2 for 10 min after 6 h of tail vein injection

of PtCo@Gem-HA-PEG NZ. Meanwhile, to evaluate the tumor growth inhibition index (TGI), the tumor volume was estimated every 7 days by the digital vernier caliper based on Eq. 5, and then TGI was calculated by Eq. 6:

$$\text{Tumor volume}\left(\text{mm}^3\right) = \frac{1}{2} \times \left(\text{lenght} \times \text{width}^2\right), \tag{5}$$

$$\text{TGI}\,(\%) = \frac{\text{mean volume of control tumors} - \text{mean volume of treated tumors}}{\text{mean volume of control tumors}} \times 100. \tag{6}$$

At the indicated time, mice were euthanized on the 35th day, and the tumors were used for histological assay after weighing and photographing.

Gem and PtCo NZ distribution

HPLC and atomic absorption methods were used to evaluate the amount of Gem and PtCo NZ in liver, spleen, lung, heart, brain, kidney, and tumor tissues, respectively. In order to determine the Gem concentration in the main tissues, tissue samples were first washed with saline and dried on filter paper. Then, the tissues were digested in acetonitrile + water with an equal volume to extract the required liquid according to the method of Zhang et al. (2010). At the end, 0.2 mL of the extracted liquid was analyzed using HPLC (SPD-M20A, Japan). Likewise, to assess the concentration of PtCo NZ, main tissue samples were digested by microwave and an acidic mixture (HNO3/HClO4, (5:1)). Each digested tissue (0.3 g) was diluted with deionized water (60 mL) and evaluated by atomic absorption spectrophotometry.

Histological assay

For the purpose of histological studies, the main organs and tumors were collected from mice after 48 h from the last injection. Harvested tumors and organs were fixed with 10% paraformaldehyde, embedded in paraffin, sectioned at 4 μm, and finally stained with H&E. Histology was performed at Tehran University College of and the samples were evaluated with an 4,559,607 Carl Zeiss microscope.

Gene expression

4T1 cells obtained from density gradient centrifugation of tumors digested by collagenase IV (Sigma-Aldrich) which obtained from control, Gem and PtCo@Gem-HA-PEG NZ were used. In the next step, Trizol reagent was used to extract total RNA from tumors (~ 100 mg) according to the manufacturer's protocols. To remove genomic DNA contamination, the RNA was treated with DNase I and cDNA was generated from 1 μg of RNA by applying reveres Aid First Strand cDNA Synthesis Kit (Biosystems™, UK). Amplification was carried out with UltraSYBR Mix (COWIN Bioscience Co., China) by applying a Stratagene Mx3005P qRT-PCR system. The specific primers are including of TNF-α (F:5′-GCTTCAACGGCACCGTGACAAT-3′ and R:5′-CTGAGTCCTGGGGGT TTGTGACATT-3′), Bcl-2 (F:5′-GAGTTCGGTGGGGTCATGTG-3′ and R:5′-CAC CTACCCAGCCTCCGTTA-3′), Caspase 9 (F:5′-CCTTCCTCTCTTCATCTCCTGCT-3′ and R:5′-TTGCTGTGAGTCCCATTGGT-3′), Caspase 7 (F:5′-CGGAGCTGGAAA

AGGTGGAT-3′ and R:5′-GGATTCATCAACGAACGGCG-3′), Caspase 3 (F:5′-CTT GTGAGTTCTGGTTTGTGTGG-3′ and R:5′-GATGCTTTCCAAGTCCTGTGTG-3′) and β-Actin (F:5′-AATTCCATCATGAAGTGTGA-3′ and R:5′-ACTCCTGCTTGCTGA TCCAC-3′). Gene expression was normalized using β-actin as the reference gene under the following reaction situations: 95 °C for 15 s, 60 °C for 60 s, and 72 °C for 30 s. The specific gene expression value was applied by calculating $2^{-\Delta\Delta Ct}$.

Statistical analysis

GraphPad Prism 7 was used for statistical analysis. All the data were reported as mean ± standard error of means. The differences between groups were evaluated by one-way analysis of variance and Student's t-test. $P < 0.05$ were considered as statistical significance.

Results

Fabrication and characterization of PtCo@Gem-HA-PEG

As shown in Fig. 2A, HA reacted with NH_2-PEG-SH in the presence of carbonyldiimidazole reagent. The change of NMR spectrum in the region of 3 to 4 ppm, especially in the region of 3.6 ppm (related to ethylene chain resonance) and 2.65 ppm region (related to amide coupling reactions) indicates the coupling reaction of the above two compounds.

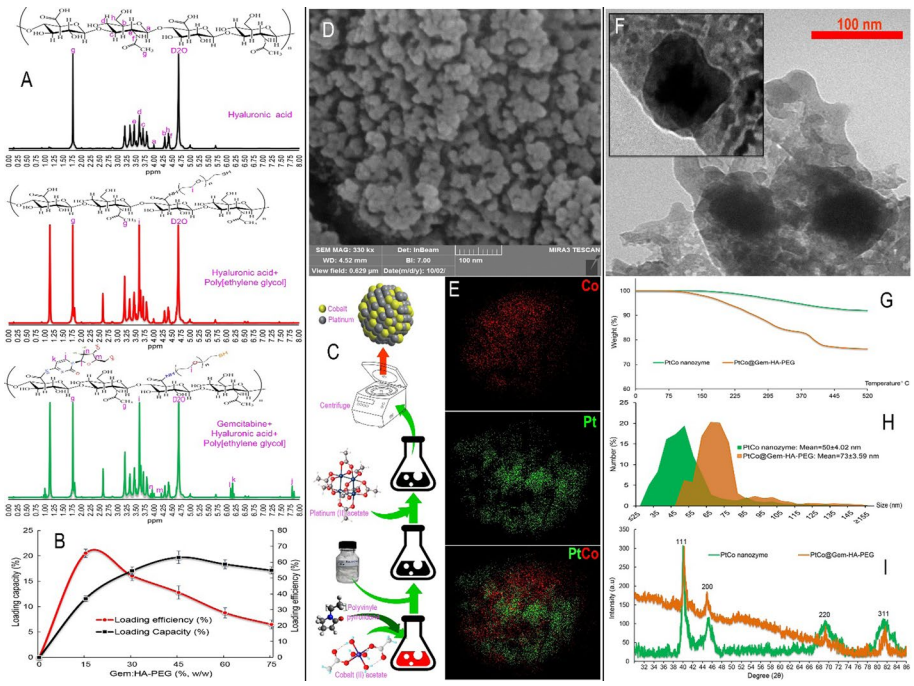

Fig. 2 **A** ^{1}HNMR spectrum of hyaluronic acid (HA), HA-(poly[ethylene glycol])PEG and gemcitabine (Gem)-HA-PEG. **B** Loading capacity% and loading efficacy%. **C** Schematic view of platinum–cobalt (PtCo) nanozyme synthesis. **D**, **E** Representative SEM image and elemental mapping of PtCo nanozyme. **F** Representative TEM image of PtCo@Gem-HA-PEG nanozyme. **G**–**I** Thermogravimetric analysis, sizes distribution, and XRD patterns of PtCo and PtCo@Gem-HA-PEG

On the other hand, the change of signals in the regions of 3.9, 4.2, 6.15, 6.2 and 7.8 ppm in Gem-HA-PEG confirms the loading of Gem in HA-PEG polymer. In the following, it was revealed that HA-PEG has a high loading capacity (%) for Gem loading (Fig. 2B), but the loading efficiency (%) output shows that despite the solubility of Gem in water, its amount decreases with the rise of drug concentration. Thus, the optimal point of Gem concentration used in loading based on the loading capacity (17.05%) and the loading efficiency (51.04%) is 60 mg per 200 mg of HA-PEG (Fig. 2B).

PtCo NZ based on a reduction strategy were synthesized via the addition of Pt to Co-B-O complex intermediates at room temperature (Fig. 2C). Scanning Electron Microscope (SEM) images (Fig. 2D) show a relatively uniform morphology with a size of 40–60 nm, while dynamic light scattering (DLS) output confirmed the size of PtCo NZ with dimensions of ~ 50 nm (Fig. 2H). In addition, TEM and DLS results exhibited Gem-HA-PEG deposition on PtCo NZ with increasing particle size from ~ 50 nm to ~ 73 nm. Also, TGA confirmed thiol-containing Gem-HA-PEG on PtCo NZ by showing a 15% reduction in the weight of the PtCo@Gem-HA-PEG (Fig. 2G). In this regard, the change in the main diffraction intensity of the XRD peaks at 39.9° (111), 44.2° (200), 69.9° (220) and 82.1° (311) confirms the presence of Gem-HA-PEG on PtCo NZ (Fig. 2I).

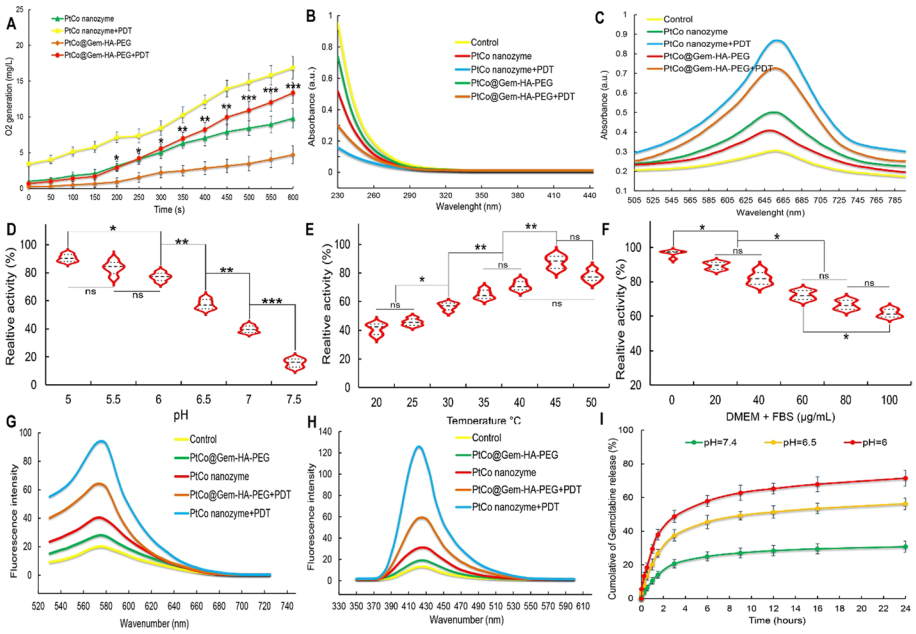

Fig. 3 **A** O_2 generation in H2O2 solution with different concentrations of platinum–cobalt (PtCo) nanozyme with and without photodynamic therapy (PDT) and platinum–cobalt@gemcitabine-hyaluronic acid (HA)-poly[ethylene glycol] (PtCo@Gem-HA-PEG) with and without PDT. **B**, **C** The studies of catalase-like and peroxidase-like activities of with different treatments. **D**–**F** The influence of pH, temperature and physiological proteins on catalytic ability of PtCo@Gem-HA-PEG nanozyme. **G**, **H** Fluorescence spectra of hydroethidine and terephthalic acid incubated with PtCo@Gem-HA-PEG in the hypoxic condition to show the presence of $O_2^{\bullet-}$ and $^{\bullet}OH$, respectively. **I** Quantitative analyses of Gem release from PtCo@Gem-HA-PEG at 37 °C with 1 mM H_2O_2 and different pH. $^{*}P < 0.05$, $^{**}P < 0.01$, and $^{***}P < 0.001$ indicate significant differences

The ability of PtCo@Gem-HA-PEG catalytic activities

Figure 3A based on O_2 generation reveals that the PtCo NZ designed with and without PDT has catalase activity in the presence of H_2O_2. While the use of Gem-HA-PEG as a coating decreased the catalase activity of PtCo NZ. However, the catalase activity of PtCo@Gem-HA-PEG NZ is significantly enhanced by using PDT (Fig. 3A). In confirmation of this finding, the decrease in H_2O_2 level indicates the catalysis activity of PtCo NZ and PtCo@Gem-HA-PEG NZ, which the application of PDT reduces the level of H_2O_2 in a more obvious way (Fig. 3B). Therefore, it seems that the destruction of the Gem-HA-PEG coating in the lysosome of the TNBC cells increases the possibility of O_2 generation, especially in PDT. Meanwhile, the results of Fig. 3C also show the capability of peroxidase-like activity in PtCo NZ and PtCo@Gem-HA-PEG NZ based on TMB catalysis in the presence of H_2O_2. Despite the increase in the peroxidase-like activity of PtCo NZ and PtCo@Gem-HA-PEG NZ synergized with PDT, the results of Fig. 3 appearance that the peroxidase-like activity of NZ is dependent on the pH and temperature of the environment. The results show a significant increase in the enzymatic activity of PtCo@Gem-HA-PEG NZ in pH below 6.5 and temperature 35 to 45 °C. Therefore, the acidity of the tumor microenvironment (with a pH between 6.2 and 7) along with its temperature (between 37 and 39 °C) can enhance the performance of PtCo@Gem-HA-PEG NZ. Meanwhile, Fig. 3F displays the stability of catalytic activity (above 60%) of PtCo@Gem-HA-PEG NZ in physiological conditions containing various proteins, which can be a guarantee of PtCo@Gem-HA-PEG NZ activity inside the cell. Since the activity of NZ in the treatment of tumors is generally evaluated by the production of radicals, the results of Fig. 3G and 3H, respectively, based on the increase in the fluorescence intensity of hydroethidine and 2-hydroxyterephthalic acid, confirmed that PtCo@Gem-HA-PEG NZ, effectively produces $O2^{\bullet-}$ and $^{\bullet}OH$, especially with synergistic activity of PDT.

Drug release from PtCo@Gem-HA-PEG

The release rate of Gem at pH 6.0, 6.5 and 7.4 illustrations that the drug release profile is time dependent. The highest release level of Gem in pH 6 and 6.5 were 71.1% and 56.3% compared to the control. The release rate of Gem at pH 6.0, 6.5 and 7.4 shows that the drug release profile is time dependent. Sensitivity to environmental acidity in Gem release is considered an ideal system because the tumor microenvironment has a relatively acidic environment (pH 6.0 to 6.5) (Khan et al. 2021). It seems that increasing the acidity of the environment by weakening and degrading the amide bonds located in Gem-HA-PEG greatly accelerates the release rate of the drug. Therefore, based on NZ being sensitive to environmental pH, it can be hoped that the drug will be less loaded in normal tissues with pH higher than 6.9.

In vitro activities with PtCo@Gem-HA-PEG

As can be seen in Fig. 4A, B, the synergism of chemotherapy by PtCo@Gem-HA-PEG NZ with PDT by laser irradiation (660 nm, 30 mW/cm^2 for 10 min) on cancerous cells causes the greatest toxicity in 4T1 cells compared to other groups. Despite the increase in toxicity with increasing doses of PtCo@Gem-HA-PEG or bare Gem, the toxicity results show that there is no significant difference between PtCo@Gem-HA-PEG NZ with PtCo@Gem-HA-PEG NZ + PDT or PtCo@Gem-HA-PEG NZ with bare Gem

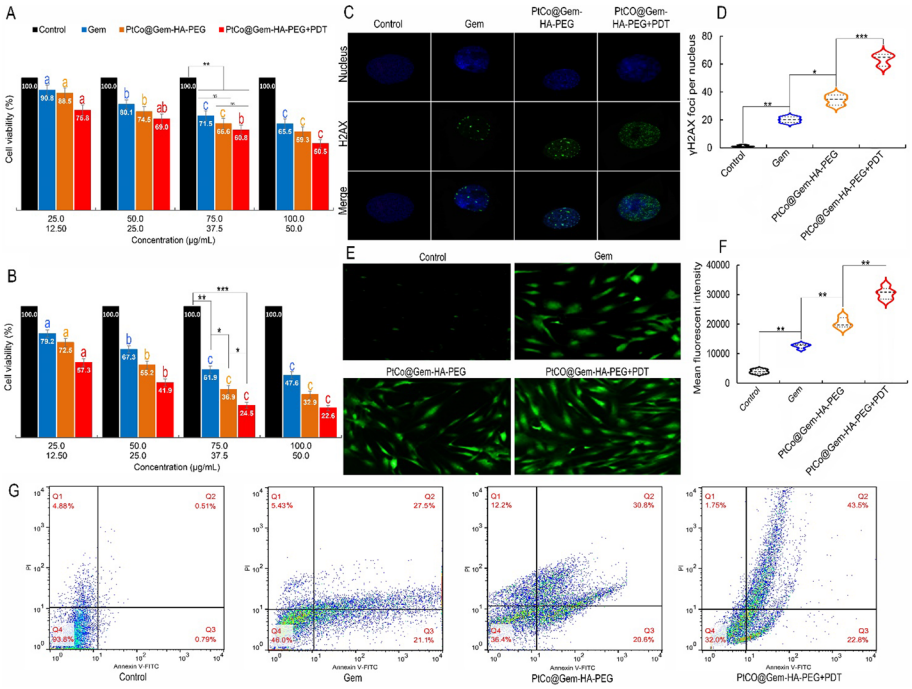

Fig. 4 Cell viability of 4T1 cells treated with Gemcitabine (Gem) (12.5, 25, 37.5 and 50 μg/mL), platinumCobalt@Gem-hyaluronic acid (HA)-poly[ethylene glycol] (PtCo@Gem-HA-PEG) with and without photodynamic therapy (PDT) (25, 50, 75 and 100 μg/mL) at 24 (**A**) and 48 (**B**) hours of incubation. **C**, **D** γ-H2AX foci immunofluorescence staining and number of foci per nucleous of 4T1 cells incubated in different treatments. The scale bar is 20 μm. **E**, **F** Representative DCF staining images of 4T1 cells and mean fluorescent intensity in different treatments for ROS evaluation. The scale bar is 60 μm. **G** Annexin V and PI staining assays of 4T1 cells treated in different treatments. Different letters a, b and c are significantly different at $P < 0.05$. $^{*}P < 0.05$, $^{**}P < 0.01$, and $^{***}P < 0.001$ indicate significant differences

groups in the applied concentrations. Nevertheless, increasing the time of presence of PtCo@Gem-HA-PEG NZ with and without PDT and Gem in the culture medium from 24 to 48 h caused significant toxicity between different groups. Therefore, the toxicity of NZ with and without PDT depends on the duration of their presence in the environment in addition to the dosage. On the other hand, genomic damage caused by applying Gem with and without nanocarriers based on γ-H2AX immunofluorescence staining in Fig. 4C confirms that the use of PtCo@Gem-HA-PEG NZ compared to bare Gem will have more destructive effects on 4T1 cells compared to bare Gem through DNA damage. Likewise, the synergistic activity of PtCo@Gem-HA-PEG NZ with PDT increases the intensity of damage to 4T1 cancer cells more than 1.5 and 2 times compared to PtCo@Gem-HA-PEG NZ and bare Gem (Fig. 4D). In this line, the results of ROS generation based on the increase of 2.45 and 1.43 times green fluorescent intensity in PtCo@Gem-HA-PEG NZ + PDT group compared to bare Gem and PtCo@Gem-HA-PEG NZ, respectively, indicate the high effectiveness of chemotherapy combined with PDT in removing 4T1 cells (Fig. 4E, F). In the following, the output of Fig. 4A and J confirmed that compared to bare Gem, PtCo@Gem-HA-PEG has a more significant toxicity due to its higher capacity in intracellular ROS formation and increased level of apoptosis in Q2 (late apoptosis) and Q3 (early apoptosis) regions. The synergistic activity of PtCo@

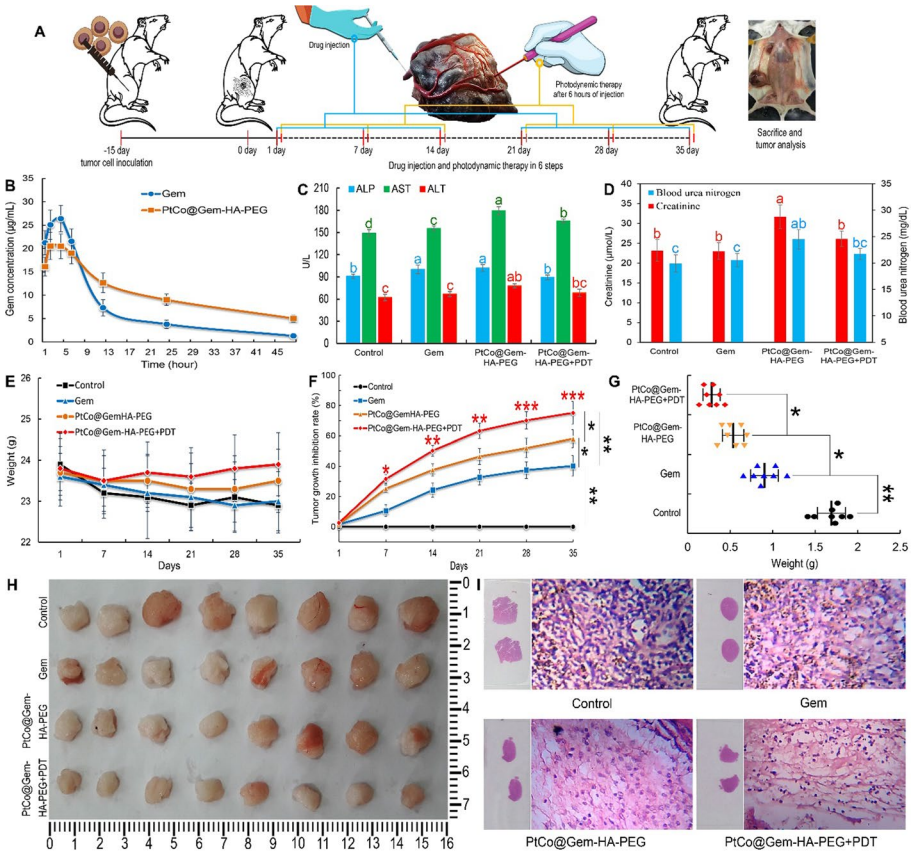

Fig. 5 **A** Schematic view of the treatment process of mice with triple-negative breast cancer cells. **B** Gemcitabine (Gem) concentration in blood in Gem and platinumCobalt@Gem-hyaluronic acid (HA)-poly[ethylane glycol] (PtCo@Gem-HA-PEG) groups. **C** Comparison of liver factors include of Alanine transaminase (ALT), aspartate aminotransferase (AST), alkaline phosphatase (ALP) and **D** kidney factors include of blood urea nitrogen (BUN) and creatinine (CRA) in control, Gem, PtCo@Gem-HA-PEG with and without photodynamic therapy (PDT) groups. **E** Weight of mice during 35-day treatment. **F** Tumor growth inhibition curve in each group after different treatments. **G** Tumor weight and **H** its digital photographs recorded from each group. **I** Histological observation of treated tumor tissues visualized using H&E staining (Scale bars are 100 μm.). Different letters a, b and c are significantly different at $P < 0.05$. $^{*}P < 0.05$, $^{**}P < 0.01$, and $^{***}P < 0.001$ indicate significant differences

Gem-HA-PEG with PDT not only increased the intracellular ROS in an outstanding way, but also shifted the increased approach of apoptosis from Q3 region to Q2 (Fig. 4F and J).

In vivo activities with PtCo@Gem-HA-PEG

In addition to in vitro evaluations, toxicological and therapeutic evaluations of bare Gem and PtCo@Gem-HA-PEG NZ with and without PDT were performed on mice based on schematic process Fig. 5A. After the intravenous tail injection of bare Gem and PtCo@Gem-HA-PEG NZ, the drug distribution in the blood at different times shows that the highest level of Gem release in the blood at the initial time corresponds to the bare Gem (Fig. 5B). While the lowest clearance of Gem based on its more stable presence in the blood belongs to the PtCo@Gem-HA-PEG NZ. Therefore, the higher circulating profile

of Gem by PtCo@Gem-HA-PEG NZ can provide the possibility of their presence in the tumor. Nevertheless, the results of Fig. 5C show that the presence of PtCo@Gem-HA-PEG NZ for more stable Gem in the blood significantly increases liver markers including ALP, AST and ALT compared to bare Gem and the control groups. Likewise, kidney markers including BUN and CRA are increased by using PtCo@Gem-HA-PEG NZ (Fig. 5D). In the following, it was determined that the use of bare Gem and PtCo@Gem-HA-PEG NZ with and without PDT had no effect on the weight of mice compared to the control (Fig. 5E). But, the synergy of PtCo@Gem-HA-PEG NZ with PDT effectively prevented the development of tumors compared to other groups (Fig. 5F). In confirmation of this finding, after collecting the tumors, it was observed that the weight of the tumors in the PtCo@Gem-HA-PEG NZ group was significantly reduced compared to the control and bare Gem (Fig. 5 G); whereas, the application of PDT with PtCo@Gem-HA-PEG NZ has significantly reduced the weight of tumors compared to other groups (Fig. 5G, H).

In the antitumor activities of PtCo@Gem-HA-PEG NZ, it was revealed that despite the favorable accumulation of Gem in tumor tissue and their significant reduction in main tissues (Fig. 6A), the accumulation of PtCo@Gem-HA-PEG NZ in the main tissues, especially the liver, spleen, and lung (Fig. 6B), increases the possibility of side

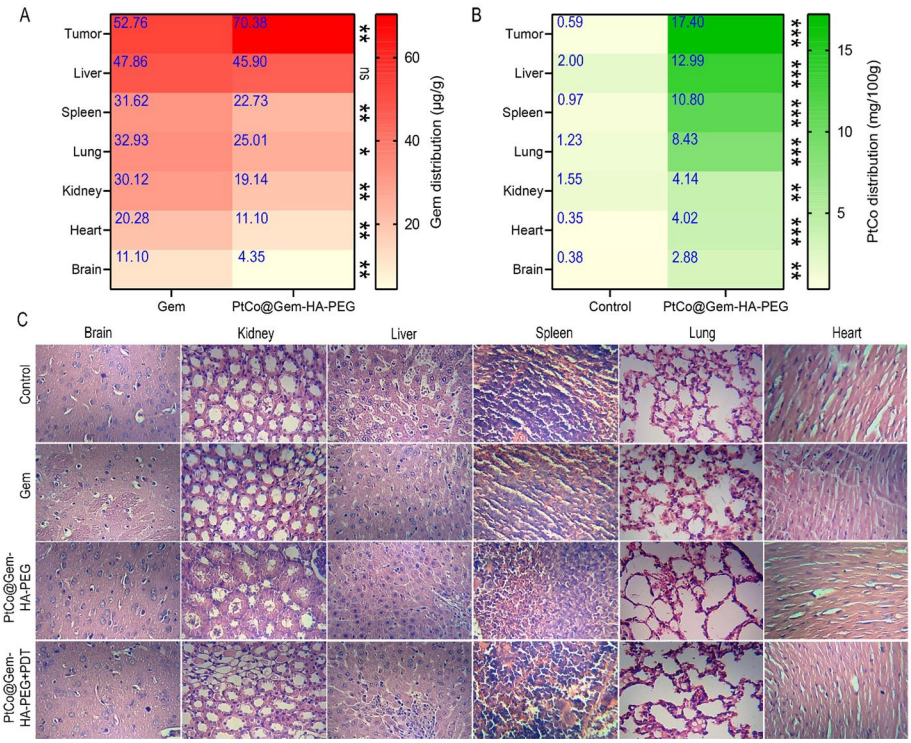

Fig. 6 **A** Gemcitabine (Gem) and **B** platinum–cobalt nanozyme concentrations in tumor, liver, spleen, lung, kidney, heart and brain tissues in the Gem and platinumCobalt@Gem-hyaluronic acid (HA)-poly[ethylene glycol] (PtCo@Gem-HA-PEG) groups. **C** Histological investigations through H&E staining of main organs include of brain, kidney, liver, spleen, lung and heart after 35 days of treatment with Gem and PtCo@Gem-HA-PEG NZ with and without PDT. Scale bars are 100 μm. $^{*}P < 0.05$, $^{**}P < 0.01$, $^{***}P < 0.001$ and $^{****}P < 0.0001$ indicate significant differences (ns: non-significant)

effects; whereas, synergized PtCo@Gem-HA-PEG NZ with PDT significantly reduced the weight of tumors compared to other groups (Fig. 5G, H). In this regard, the histological results in Fig. 6C show that morphological changes such as increased fibrosis in the parenchyma of liver tissue, shrinking of liver cells, increased heterochromatin nuclei (decrease in nuclear activity) and removal of the nucleus in some liver cells in the PtCo@Gem-HA-PEG NZ is considerable. Similarly, removing the nucleus of some kidney cells, increasing the thickness of renal tubules and reducing the internal diameter of the ducts, tearing of some renal tubules, destruction of tissue integrity and tissue inflammation in kidney tissue can be seen in PtCo@Gem-HA-PEG NZ. In addition, NZ in the lung caused the destruction of the cell membrane and rupture of the air sacs. Moreover, primary damage caused by PtCo accumulation in spleen tissue can be followed. Meanwhile, the use of PtCo@Gem-HA-PEG NZ combined with PDT has effectively reduced the level of damage. However, the morphological changes of TNBC tissue including of cytoplasmic loosening, destruction of tissue integrity, and nuclear condensation along with removal of the nucleus in some tumor cells caused by PtCo@Gem-HA-PEG NZ, especially in the synergistic activity with PDT, are promising (Fig. 5I).

The evaluation of the apoptosis mechanism in Fig. 7 shows the high effectiveness of PtCo@Gem-HA-PEG NZ combined with PDT in inducing the apoptosis in both intrinsic and extrinsic processes. In this way that the synergy of PtCo@Gem-HA-PEG NZ with PDT causes an increase in the relative expression of TNF-α and Caspase-7 associated with the extrinsic pathway of apoptosis, and decrease/increase in relative

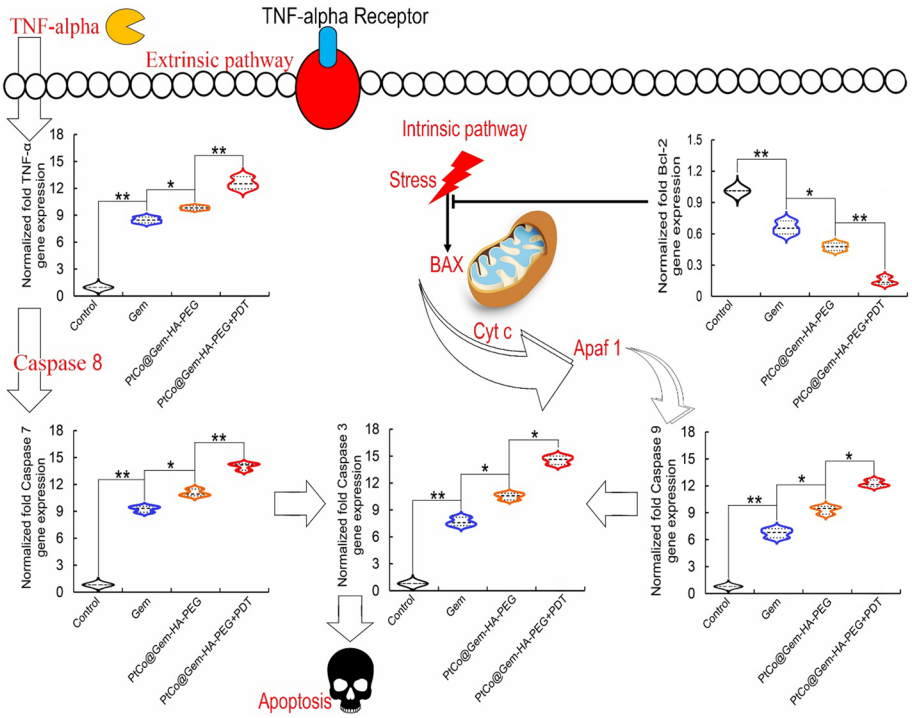

Fig. 7 The effect of gemcitabine (Gem), platinum–cobalt@Gem-hyaluronic acid (HA)-poly[ethylene glycol] (PtCo@Gem-HA-PEG) with and without photodynamic therapy (PDT) on the extrinsic and intrinsic mechanisms of apoptosis by examining the expression of TNF-α, Caspase-7, Bcl-2, Caspase-9, and Caspase-3 in triple-negative breast cancer cells. $^{*}P<0.05$, $^{**}P<0.01$, and $^{***}P<0.001$ indicate significant differences

expression of Bcl-2/Caspase-9 related to the internal pathway of apoptosis. In the following, synergized PtCo@Gem-HA-PEG NZ with PDT irreversibly leads to tumoral cell death through a 1.5- and twofold increase in Caspase-3 compared to other groups (Fig. 7). Taken together, these results show that combined therapeutic activities induce higher apoptosis in TNBC cell.

Discussion

The PtCo NZ is of great interest compared to other peroxidase–catalase mimics due to their easy preparation, high catalytic ability in a wide pH and temperature range, tunable size, good stability, and favorable response to PDT (Hao et al. 2020; Ren et al. 2022). Despite the favorable effects of PtCo NZ synthesized with the same atomic ratio (1:1), there have been reports indicating higher catalytic effects of Pt:Co atomic ratio 3:1 in NZ (Wei et al. 2020; Zhang et al. 2018). However, the increase of catalytic activity is not considered a special indicator in therapeutic activities due to the increased possibility of toxicity in non-target tissues with long-term presence. Nevertheless, the increased catalysis activity of NZ, which in tumors can reduce the level of hypoxia for greater drug penetration (Jiao et al. 2021; Zhu et al. 2020; Wang et al. 2020), was a criterion for enhancing the catalytic activity of PtCo@Gem-HA-PEG NZ by PDT (Fig. 3A, B). Although the rate of O_2 generation in this research (Fig. 3A), similar to the study of Wang et al. (2018), was lower than the report of Nie et al. (2022) and Bao et al. (2021), the catalase- and peroxidase-like activities of PtCo@Gem-HA-PEG NZ enhanced with PDT effectively reduced the level of hypoxia (Fig. 3G, H). Therefore, the use of PtCo@Gem-HA-PEG NZ with enzymatic dual behavior that shows stable enzyme activity in a wide range of pH, temperature and physiological conditions (Fig. 3D–F) can not only guarantee the reduction of hypoxia, but also lead to more effective treatment of TNBC through $O_2^{\bullet -}$ generation. Although in this research it was not determined which radicals type will be more effective in therapeutic activity, but in hypoxic conditions rich in H_2O_2, is conceivable $O_2^{\bullet -}$ and $^{\bullet}OH$ generation by synergized PtCo@Gem-HA-PEG NZ with PDT (Fig. 3G, H), in agreement with Zeng et al. (2023) and Jiao et al. (2021). In this line, by proving the competence of PtCo@Gem-HA-PEG NZ, especially in synergistic activity with PDT in causing toxicity on 4T1 cells (Fig. 4B) through enhancing intracellular ROS (Fig. 4E–G) and raising the production of nuclear foci (Fig. 4D) caused by DNA breakage that is likely related to the radicals produced and the concentration of Gem in nucleus, can improve the treatment of TNBC. The increasing fluorescence intensity in hypoxic conditions indicates the dominance of PtCo@Gem-HA-PEG NZ over hypoxia and the production of ROS even in deep tissues, that tissue depth is limiting PDT activity (Sun et al. 2022).

In the in vivo activities, it was found that the higher circulating activity of PtCo@Gem-HA-PEG NZ in the blood (Fig. 5B) could enhance the presence of Gem in the TNBC based on the EPR approach (Sharifi et al. 2022), which is confirmed by the results of Fig. 6A, B. In addition, based on the type of Gem release diagram in the blood, it seems that PtCo@Gem-HA-PEG NZ follows a two-compartment model, based on the in vitro Gem release (Fig. 3I), the first compartment releases Gem as a burst release due to drug washout and the second compartment releases the drug slowly through polymer degradation. However, the more stable presence of PtCo@Gem-HA-PEG NZ to preserve Gem in the blood caused adverse changes in liver (ALT, AST, and ALP) and kidney (BUN

and CRA) factors, which indicates the damage caused to them. Despite the reduction of damage in the synergized PtCo@Gem-HA-PEG NZ with PDT, it seems that due to the high capacity of PtCo@Gem-HA-PEG NZ accumulation in main organs, especially the liver, spleen, lung, and kidney (Fig. 6B), the probability of damage could increase in these groups. However, the outputs of tumor status in Fig. 5F–H show that PtCo@Gem-HA-PEG NZ combined with PDT effectively prevents tumor growth and development. Increasing Gem loading in the TNBC tissue (Fig. 6A) and strengthening the production of radicals (based on the results of Fig. 4E, F) in cancerous tissue are the main reasons. While the low effectiveness of PtCo@Gem-HA-PEG NZ in stopping tumor development compared to the synergistic approach can be related to the severe hypoxic condition of the tumor and the weakness of PtCo NZ in reducing hypoxia in real condition similar to the study by Wang et al. (2018). Hence, Wang et al. (2018) added MnO_2 to the designed PtCo NZ (MnO_2@PtCo) and achieved high success in stopping tumor growth due to the excellent ability of manganese oxide to reduce hypoxia. Despite the report of the non-toxicity of MnO_2@PtCo NZ in main tissues by Wang et al. (2018) during 14 days, this research revealed that the long-term presence of PtCo@Gem-HA-PEG NZ (35 days) can cause damage to liver and kidney tissue (based on the results of Figs. 5C, D and 6C), despite the expected damage in cancerous tissue (Fig. 5I). Based on the results of Liu et al. (2020), Li et al. (2018) and Wang et al. (2018), it seems that the accumulation of NZ in non-target tissues in the long term and the increase in catalytic activity for the production of ROS are the main factors in the occurrence of toxicity. Therefore, regardless of the type of NZ, it seems that the use of production approaches to reduce the accumulation of NZ in non-target tissues such as reducing particle size, using coatings to reduce or stop their catalytic activity, and increasing their loading in cancerous tumors is considered as a vital activity.

Conclusion

In this research, by designing a combined treatment platform based on NZ obtained by integrating Pt and Co with HA-PEG coating containing Gem and synergistic activity with PDT, the following objectives were investigated: (1) intrinsic properties of PtCo@Gem-HA-PEG NZ to produce $O_2^{\bullet-}$ and $^{\bullet}OH$ in hypoxic conditions; (2) effects of PtCo@Gem-HA-PEG NZ toxicity on 4T1 cells based on the state of the nucleus and ROS accumulation in the cells; (3) drug distribution in blood and vital tissues; (4) toxicology of PtCo@Gem-HA-PEG NZ on main tissues, and (5) tumor status and apoptosis induction pathways in them. By integrating drug delivery and catalytic activities enhanced with PDT, PtCo@Gem-HA-PEG NZ had excellent antitumor properties in vitro and in vivo without reducing the weight of mice. Higher drug loading in cancer tissues and strengthening of apoptosis stimulating factors in cancerous cells, along with increasing the drug's retention time in the blood, the hopes of TNBC treatment were strengthened by synergized PtCo@Gem-HA-PEG NZ with PDT. Nevertheless, the occurrence of toxicity in the liver and kidney tissues and the change in their function challenges the path of using PtCo@Gem-HA-PEG NZ in therapeutic activities. It seems, this study provides

a clear concept of the effectiveness of antitumor activities of NZ and its mechanism in the treatment of TNBC with possible toxicities.

Acknowledgements
The statements made herein are the sole responsibility of the authors.

Author contributions
MS, RK, MA: conceptualization, methodology, revision; MS, MA: analysis, validation, supervision; writing. All authors read and approved the final manuscript.

Availability of data and materials
The datasets used and analyzed during the current study are available from the corresponding author on reasonable request.

Declarations

Ethics approval and consent to participate
All animal use procedures were carried out in accordance with the Regulations of Animal Care and Use Committee of Shahroud University of Medical Sciences, with the approval of the Ethics Committee in our University.

Consent for publication
All authors read and approve the final manuscript.

Competing interests
All of the authors declare that they have no conflict of interest.

Received: 6 January 2023 Accepted: 12 April 2023
Published online: 24 April 2023

References

Aggarwal S, Gupta S, Pabla D, Murthy R (2013) Gemcitabine-loaded PLGA-PEG immunonanoparticles for targeted chemotherapy of pancreatic cancer. Cancer Nanotechnol 4:145–157
Alsughayer AM, Dabbagh TZ, Abdel-Razeq RH, Al-Jussani GN, Alhassoon S, Sughayer MA (2022) Changing trends in estrogen receptors/progesterone receptors/human epidermal growth factor receptor 2 prevalence rates among Jordanian patients with breast cancer over the years. JCO Global Oncology 8:e2100359
Bao Z, Li K, Hou P, Xiao R, Yuan Y, Sun Z (2021) Nanoscale metal–organic framework composites for phototherapy and synergistic therapy of cancer. Mater Chem Front 5:1632–1654
Bao J, Wang Y, Li C, Yang C, Xu H, Liang Q, Zhou Y, Zhang L, He Y, Tong H et al (2022) Gold-promoting-satellite to boost photothermal conversion efficiency of Cu2-xSe for triple-negative breast cancer targeting therapy. Mater Today Nano 18:100211
Cen J, Huang Y, Liu J, Liu Y (2022) Thermo-responsive palladium–ruthenium nanozyme synergistic photodynamic therapy for metastatic breast cancer management. J Mater Chem B 10:10027
Falahati M, Sharifi M, Ten Hagen TL (2022) Explaining chemical clues of metal organic framework-nanozyme nano-/micro-motors in targeted treatment of cancers: benchmarks and challenges. J Nanobiotechnol 20:1–26
Fan Y, Wang Q, Lin G, Shi Y, Gu Z, Ding T (2017) Combination of using prodrug-modified cationic liposome nanocomplexes and a potentiating strategy via targeted co-delivery of gemcitabine and docetaxel for CD44-overexpressed triple negative breast cancer therapy. Acta Biomater 62:257–272
Gao Z, Li Y, Zhang Y, Cheng K, An P, Chen F, Chen J, You C, Zhu Q, Sun B (2020) Biomimetic platinum nanozyme immobilized on 2D metal-organic frameworks for mitochondrion-targeting and oxygen self-supply photodynamic therapy. ACS Appl Mater Interfaces 12:1963–1972
Hao Y, Chen Y, He X, Yu Y, Han R, Li Y, Yang C, Hu D, Qian Z (2020) Polymeric nanoparticles with ROS-responsive prodrug and platinum nanozyme for enhanced chemophotodynamic therapy of colon cancer. Adv Sci 7:2001853
Hou G, Qian J, Guo M, Xu W, Wang J, Wang Y, Suo A (2022) Copper coordinated nanozyme-assisted photodynamic therapy for potentiating PD-1 blockade through amplifying oxidative stress. Chem Eng J 435:134778
Iqbal H, Razzaq A, Uzair B, Ul Ain N, Sajjad S, Althobaiti NA, Albalawi AE, Menaa B, Haroon M, Khan M (2021) Breast cancer inhibition by biosynthesized titanium dioxide nanoparticles is comparable to free doxorubicin but appeared safer in BALB/c mice. Materials 14:3155
Jiao J, Lu H, Wang S (2021) Photo-responsive prodrug nanoparticles for efficient cytoplasmic delivery and synergistic photodynamic-chemotherapy of metastatic triple-negative breast cancer. Acta Biomater 126:421–432
Khan S, Vahdani Y, Hussain A, Haghighat S, Heidari F, Nouri M, Bloukh SH, Edis Z, Babadaei MMN, Ale-Ebrahim M (2021) Polymeric micelles functionalized with cell penetrating peptides as potential pH-sensitive platforms in drug delivery for cancer therapy: a review. Arab J Chem 14:103264
Li J, Zu X, Liang G, Zhang K, Liu Y, Li K, Luo Z, Cai K (2018) Octopod PtCu nanoframe for dual-modal imaging-guided synergistic photothermal radiotherapy. Theranostics 8:1042
Liu Z, Xie L, Qiu K, Liao X, Rees TW, Zhao Z, Ji L, Chao H (2020) An ultrasmall RuO2 nanozyme exhibiting multienzyme-like activity for the prevention of acute kidney injury. ACS Appl Mater Interfaces 12:31205–31216

Lønning PE, Nikolaienko O, Pan K, Kurian AW, Eikesdal HP, Pettinger M, Anderson GL, Prentice RL, Chlebowski RT, Knappskog S (2022) Constitutional BRCA1 methylation and risk of incident triple-negative breast cancer and high-grade serous ovarian cancer. JAMA Oncol 8:1579–1587
Mansur AAP, Mansur HS, Leonel AG, Carvalho IC, Lage MCG, Carvalho SM, Krambrock K, Lobato ZIP (2020) Supramolecular magnetonanohybrids for multimodal targeted therapy of triple-negative breast cancer cells. J Mater Chem B 8:7166–7188
Nie Z, Vahdani Y, Cho WC, Bloukh SH, Edis Z, Haghighat S, Falahati M, Kheradmandi R, Jaragh-Alhadad LA, Sharifi M (2022) 5-Fluorouracil-containing inorganic iron oxide/platinum nanozymes with dual drug delivery and enzyme-like activity for the treatment of breast cancer. Arab J Chem 15:103966
Paroha S, Verma J, Dubey RD, Dewangan RP, Molugulu N, Bapat RA, Sahoo PK, Kesharwani P (2021) Recent advances and prospects in gemcitabine drug delivery systems. Int J Pharm 592:120043
Pellegrino B, Cavanna L, Boggiani D, Zamagni C, Frassoldati A, Schirone A, Caldara A, Rocca A, Gori S, Piacentini F (2021) Phase II study of eribulin in combination with gemcitabine for the treatment of patients with locally advanced or metastatic triple negative breast cancer (ERIGE trial). Clinical and pharmacogenetic results on behalf of the Gruppo Oncologico Italiano di Ricerca Clinica (GOIRC). ESMO Open 6:100019
Ren Q, Yu N, Wang L, Wen M, Geng P, Jiang Q, Li M, Chen Z (2022) Nanoarchitectonics with metal–organic frameworks and platinum nanozymes with improved oxygen evolution for enhanced sonodynamic/chemo-therapy. J Colloid Interface Sci 614:147–159
Sharifi M, Hosseinali SH, Yousefvand P, Salihi A, Shekha MS, Aziz FM, JouyaTalaei A, Hasan A, Falahati M (2020) Gold nanozyme: biosensing and therapeutic activities. Mater Sci Eng, C 108:110422
Sharifi M, Bai Q, Babadaei MMN, Chowdhury F, Hassan M, Taghizadeh A, Derakhshankhah H, Khan S, Hasan A, Falahati M (2021) 3D bioprinting of engineered breast cancer constructs for personalized and targeted cancer therapy. J Control Release 333:91–106
Sharifi M, Cho WC, Ansariesfahani A, Tarharoudi R, Malekisarvar H, Sari S, Bloukh SH, Edis Z, Amin M, Gleghorn JP (2022) An updated review on EPR-based solid tumor targeting nanocarriers for cancer treatment. Cancers 14:2868
Sun B, Rahmat JNB, Zhang Y (2022) Advanced techniques for performing photodynamic therapy in deep-seated tissues. Biomaterials 291:121875
Vogus DR, Evans MA, Pusuluri A, Barajas A, Zhang M, Krishnan V, Nowak M, Menegatti S, Helgeson ME, Squires TM, Mitragotri S (2017) A hyaluronic acid conjugate engineered to synergistically and sequentially deliver gemcitabine and doxorubicin to treat triple negative breast cancer. J Control Release 267:191–202
Wang Z, Zhang Y, Ju E, Liu Z, Cao F, Chen Z, Ren J, Qu X (2018) Biomimetic nanoflowers by self-assembly of nanozymes to induce intracellular oxidative damage against hypoxic tumors. Nat Commun 9:1–14
Wang D, Wu H, Phua SZF, Yang G, Lim WQ, Gu L, Qian C, Wang H, Guo Z, Chen H (2020) Self-assembled single-atom nanozyme for enhanced photodynamic therapy treatment of tumor. Nat Commun 11:1–13
Wang Y, Iqbal H, Ur-Rehman U, Zhai L, Yuan Z, Razzaq A, Lv M, Wei H, Ning X, Xin J (2022) Albumin-based nanodevices for breast cancer diagnosis and therapy. J Drug Deliv Sci Technol. 104072.
Wei M, Huang L, Huang S, Chen Z, Lyu D, Zhang X, Wang S, Tian ZQ, Shen PK (2020) Highly efficient Pt-Co alloy hollow spheres with ultra-thin shells synthesized via Co-BO complex as intermediates for hydrogen evolution reaction. J Catal 381:385–394
Wengner AM, Scholz A, Haendler B (2020) Targeting DNA damage response in prostate and breast cancer. Int J Mol Sci 21:8273
Wu M, Chen T, Wang L, Akakuru OU, Ma X, Xu J, Hu J, Chen J, Fang Q, Wu A, Li Q (2022) The strategy of precise targeting and in situ oxygenating for enhanced triple-negative breast cancer chemophototherapy. Nanoscale 14:8349–8361
Xi J, Wang Y, Gao X, Huang Y, Chen J, Chen Y, Fan L, Gao L (2022) Reverse intratumor bacteria-induced gemcitabine resistance with carbon nanozymes for enhanced tumor catalytic-chemo therapy. Nano Today 43:101395
Xie X, Lee J, Liu H, Pearson T, Lu AY, Tripathy D, Devi GR, Bartholomeusz C, Ueno NT (2021) Birinapant enhances gemcitabine's antitumor efficacy in triple-negative breast cancer by inducing intrinsic pathway-dependent apoptosis synergistic effect of birinapant and gemcitabine in TNBC. Mol Cancer Ther 20:296–306
Xing L, Liu X-Y, Zhou T-J, Wan X, Wang Y, Jiang H-L (2021) Photothermal nanozyme-ignited Fenton reaction-independent ferroptosis for breast cancer therapy. J Control Release 339:14–26
Yardley D, Coleman R, Conte P, Cortes J, Brufsky A, Shtivelband M, Young R, Bengala C, Ali H, Eakel J (2018) nab-Paclitaxel plus carboplatin or gemcitabine versus gemcitabine plus carboplatin as first-line treatment of patients with triple-negative metastatic breast cancer: results from the tnAcity trial. Ann Oncol 29:1763–1770
Zeng Z, Wang Z, Chen S, Xiao C, Liu M, Zhang J, Fan J, Zhao Y, Liu B (2022) Bio-nanocomplexes with autonomous O2 generation efficiently inhibit triple negative breast cancer through enhanced chemo-PDT. J Nanobiotechnol 20:1–18
Zeng X, Ruan Y, Chen Q, Yan S, Huang W (2023) Biocatalytic cascade in tumor microenvironment with a Fe2O3/Au hybrid nanozyme for synergistic treatment of triple negative breast cancer. Chem Eng J 452:138422
Zhang W, Shi Y, Chen Y, Yu S, Hao J, Luo J, Sha X, Fang X (2010) Enhanced antitumor efficacy by paclitaxel-loaded pluronic P123/F127 mixed micelles against non-small cell lung cancer based on passive tumor targeting and modulation of drug resistance. Eur J Pharm Biopharm 75:341–353
Zhang Y, Wang F, Liu C, Wang Z, Kang L, Huang Y, Dong K, Ren J, Qu X (2018) Nanozyme decorated metal–organic frameworks for enhanced photodynamic therapy. ACS Nano 12:651–661
Zhu D, Lyu M, Jiang W, Suo M, Huang Q, Li K (2020) A biomimetic nanozyme/camptothecin hybrid system for synergistically enhanced radiotherapy. J Mater Chem B 8:5312–5319
Zhu Y, Hu Y, Tang C, Guan X, Zhang W (2022) Platinum-based systematic therapy in triple-negative breast cancer. Biochem Biophys Acta 1877:188678

Publisher's Note